Calhoun
Institutional Archive of the Naval Postgraduate School

Calhoun: The NPS Institutional Archive

Faculty and Researcher Publications | Faculty and Researcher Publications

2009

Observations of marine stratocumulus microphysics and implications for processes controlling droplet spectra: Results from the Marine Stratus/Stratocumulus Experiment

Calhoun is a project of the Dudley Knox Library at NPS, furthering the precepts and goals of open government and government transparency. All information contained herein has been approved for release by the NPS Public Affairs Officer.

Dudley Knox Library / Naval Postgraduate School
411 Dyer Road / 1 University Circle
Monterey, California USA 93943

http://www.nps.edu/library

Observations of marine stratocumulus microphysics and implications for processes controlling droplet spectra: Results from the Marine Stratus/Stratocumulus Experiment

Jian Wang,[1] Peter H. Daum,[1] Seong Soo Yum,[2] Yangang Liu,[1] Gunnar I. Senum,[1] Miao-Ling Lu,[3] John H. Seinfeld,[3] and Haflidi Jonsson[4]

Received 25 August 2008; revised 18 May 2009; accepted 10 June 2009; published 23 September 2009.

[1] During the Marine Stratus/Stratocumulus Experiment, cloud and aerosol microphysics were measured in the eastern Pacific off the coast of northern California on board Department of Energy Gulfstream-1 in July 2005. Three cases with uniform aerosol concentration and minimal drizzle concentration were examined to study cloud microphysical behavior. For these three cases, the average droplet number concentration increased with increasing altitude, while the average interstitial aerosol concentration decreased with altitude. The data show enhanced growth of large droplets and spectral broadening in cloud parcels with low liquid water mixing ratio. Three mixing models, including inhomogeneous mixing, entity type entrainment mixing, and circulation mixing proposed in this study, are examined with regard to their influences on cloud microphysics. The observed cloud microphysical behavior is most consistent with the circulation mixing, which describes the mixing between cloud parcels with different lifting condensation levels during their circulations driven by evaporative and radiative cooling. The enhanced growth and spectrum broadening resulting from the circulation mixing reduce cloud albedo at the same liquid water path and facilitate the formation of precipitation embryos.

Citation: Wang, J., P. H. Daum, S. S. Yum, Y. Liu, G. I. Senum, M.-L. Lu, J. H. Seinfeld, and H. Jonsson (2009), Observations of marine stratocumulus microphysics and implications for processes controlling droplet spectra: Results from the Marine Stratus/Stratocumulus Experiment, *J. Geophys. Res.*, *114*, D18210, doi:10.1029/2008JD011035.

1. Introduction

[2] Low-level boundary layer clouds, such as marine stratus and stratocumulus clouds, are climatically important, as they significantly reduce the solar energy absorbed by the Earth system, reducing the heating rates when compared to cloud-free conditions [*Nicholls*, 1984; *Randall et al.*, 1984]. *Twomey* [1974] suggested that cloud albedo is modified by the characteristics of cloud condensation nuclei (CCN) available to form cloud droplets. By changing cloud microphysics including droplet size distribution and concentration, perturbations in CCN may alter the radiative properties of clouds sufficiently to impact the Earth's energy budget and thus the climate. Furthermore, cloud microphysics also impacts cloud precipitation efficiency, and consequently the lifetime and coverage of clouds [*Albrecht*, 1989]. Aside from any aerosol effects, cloud dynamics alone exerts an important effect on cloud microphysics. A fundamental understanding of cloud microphysics is necessary to interpret the magnitude of cloud feedback in response to climate change due to anthropogenic emission of greenhouse gases and aerosols.

[3] Although cloud droplets are initially produced by condensation of water vapor on CCN, condensation alone cannot, in a realistic time scale, produce drops that are sufficiently large (D_d > 50 μm) to initiate the gravitational collection process, which is essential to generate precipitable size drops (e.g., drizzle drops) in warm clouds. Because the condensational growth rate of droplet decreases as droplet size increases, the size dependence of condensational growth also leads to a narrow droplet spectrum (i.e., small standard deviation of droplet diameter), which does not promote gravitational collection [*Rogers and Yau*, 1989]. In contrast to the relatively narrow spectra predicted by condensational growth, observations often show much broader cloud droplet spectra [e.g., *Politovich*, 1993; *Martin et al.*, 1994; *Hudson and Yum*, 1997], which promote gravitational collection by providing greater differences in fall velocities. Whereas some of the observed spectral broadening is due to instrumental artifacts, discrepancies between theory and observations still exist even when instrumental artifacts are taken into consideration [*Brenguier and Chaumat*,

[1]Brookhaven National Laboratory, Upton, New York, USA.
[2]Department of Atmospheric Sciences, Yonsei University, Seoul, South Korea.
[3]Department of Environmental Science and Engineering, California Institute of Technology, Pasadena, California, USA.
[4]Center for Interdisciplinary Remotely Piloted Aircraft Studies, Naval Postgraduate School, Monterey, California, USA.

Copyright 2009 by the American Geophysical Union.
0148-0227/09/2008JD011035

2001]. A number of explanations have been advanced for the discrepancies [*Beard and Ochs*, 1993], including the role of giant CCN [*Johnson*, 1982], homogeneous mixing [*Mason and Jonas*, 1974], inhomogeneous mixing [*Baker et al.*, 1980], entity type entrainment mixing [*Telford and Chai*, 1980], turbulent internal mixing [*Cooper*, 1989; *Hudson and Svensson*, 1995], droplet clustering in cloud [*Shaw et al.*, 1998; *Chaumat and Brenguier*, 2001; *Shaw*, 2003], and stochastic condensation [*Sedunov*, 1974; *McGraw and Liu*, 2006]. Observations of actual cloud droplet spectra are important in evaluating the influential processes in cloud microphysics.

[4] In this study, the microphysics of stratocumulus clouds observed during the Marine Stratus/Stratocumulus Experiment (MASE) is analyzed. To exclude aerosol effects on cloud microphysics, we focus our analysis on three cases with uniform aerosol concentrations. The observed microphysics shows enhanced growth of large droplets and spectral broadening in cloud parcels with low liquid water mixing ratio. We examine here the extent to which cloud mixing processes are able to explain the observed microphysics. Whereas the stratocumulus clouds sampled here showed minimal drizzle concentration, the effect of mixing processes on cloud microphysics (i.e., enhanced growth of large droplets and spectral broadening) may have important implications on initiation of precipitation as well as cloud albedo.

2. Marine Stratus/Stratocumulus Experiment

[5] The Marine Stratus/Stratocumulus Experiment (MASE) field campaign was carried out in July 2005 off the coast of Monterey and Point Reyes, northern California, to study aerosol-cloud interactions in the climatically important regime of the eastern Pacific marine stratocumulus [*Lu et al.*, 2007; P. H. Daum et al., Microphysical properties of stratus/stratocumulus clouds during the 2005 Marine Stratus/Stratocumulus Experiments (MASE), manuscript in preparation, 2009]. During MASE, aerosol and cloud microphysics were measured on board the Department of Energy (DOE) Gulfstream-1 (G-1) aircraft. The aircraft, stationed at Sacramento, CA, conducted 11 research flights from 6 to 27 July 2005. Details of the measurements and flights of the aircraft are described by Daum et al. (manuscript in preparation, 2009). On the G-1, aerosol size distribution from 0.12 to $\sim$2.5 μm was measured by a Passive Cavity Aerosol Spectrometer Probe (PCASP). Cloud droplet ($\sim$1 to 50 μm) and drizzle (50 μm to 1.5 mm) size distributions were measured by a Cloud and Aerosol Spectrometer (CAS) and a Cloud Imaging Probe (CIP), respectively. Cloud liquid water content (LWC) was measured by a Gerber PVM-100 probe [*Gerber et al.*, 1994]. The PCASP was calibrated using PSL standard spheres (refractive index 1.59). On the basis of the calibration, the bin boundaries were adjusted for ammonium sulfate with a refractive index of 1.51. The PCASP sample flow was also calibrated and has an accuracy of 3%. The CAS was calibrated using both glass beads and PSL standard spheres, and the bin boundaries were set for liquid water droplets with a refractive index of 1.33. The CIP probe was calibrated with a rotating disk calibrator per the manufacturer's procedure. Before each flight, the Gerber PVM-100 probe was calibrated with a light diffusing disk following manufacturer's procedure. The PVM-100 probe is estimated to have a measurement accuracy of 5% and a measurement precision of 2%. All four instruments were operated at a time resolution of 1 Hz.

3. Observations

[6] To study the effects of dynamics on cloud microphysics, we focus our analysis on cases in which the boundary layer aerosol concentration in the area of interest was essentially uniform within each flight such that the impact of subcloud aerosol variation on cloud microphysics was negligible. Here we present three cases of multialtitude sampling of clouds carried out on 27, 18, and 20 July 2005 (27 July is listed as the first case as measurements were carried out at more altitudes inside clouds than the other two cases). Ship exhaust plumes, indicated by narrow regions with elevated aerosol and SO_2 concentrations, were occasionally observed to perturb the background of otherwise uniform aerosol concentration; data reflecting ship exhaust plumes, representing a very small fraction of total measurements for the cases, are excluded from the analysis. After ship exhaust plumes are excluded, the total concentration measured by the PCASP below clouds was 624 $\pm$ 46, 330 $\pm$ 25, and 266 $\pm$ 18 cm^{-3}, and the volume average diameter was 249 $\pm$ 9, 225 $\pm$ 10, and 277 $\pm$ 14 nm for the cases on 27, 18, and 20 July, respectively. The uncertainties are one standard deviation. The variation (defined by the standard deviation divided by the mean) is about 7% in concentration and 4–5% in volume average diameter. We note that some portion of the variation in concentration may be due to the counting statistics of PCASP. The PCASP has a sample rate of about 1 cm^3 s^{-1}. At a concentration of 300 cm^{-3}, the variation due to counting statistics is about 6%. The measurements suggest that the aerosol concentrations were quite uniform for the three cases. For each of three cases, measurements were carried out in the morning, between $\sim$9:00 and $\sim$11:00 (local time), in solid decks of stratocumulus clouds with very low drizzle number concentration and drizzle LWC. The average number concentration of drizzle measured by the CIP (defined as drops larger than 50 μm in diameter) was 0.9, 6, and 2 L^{-1}, and the average drizzle LWC was 2.5 $\times$ 10^{-4}, 3.3 $\times$ 10^{-3}, 7.2 $\times$ 10^{-4}g m^{-3} for the cases on 27, 18, and 20 July, respectively. The maximum drizzle number concentration was 7, 23, and 7 L^{-1}, and the maximum drizzle LWC was 4.6 $\times$ 10^{-3}, 2.6 $\times$ 10^{-2}, and 2.6 $\times$ 10^{-3} g m^{-3} for the cases on 27, 18, and 20 July.

[7] Figure 1 shows the 3-D flight track on 27 July 2005, colored according to time, which is typical of G-1 flight patterns during MASE. The G-1 first climbed to an altitude of $\sim$1.5 km after takeoff from Sacramento and flew west toward Point Reyes. After brief sampling at Point Reyes, the G-1 headed offshore, and flew repetitive multialtitude patterns with legs below cloud (if possible), at multiple altitudes in cloud, and above the cloud top. In this section, the vertical variations of cloud microphysical parameters and interstitial aerosol concentration, as well as the correlations among them at different sampling altitudes inside the clouds, are presented.

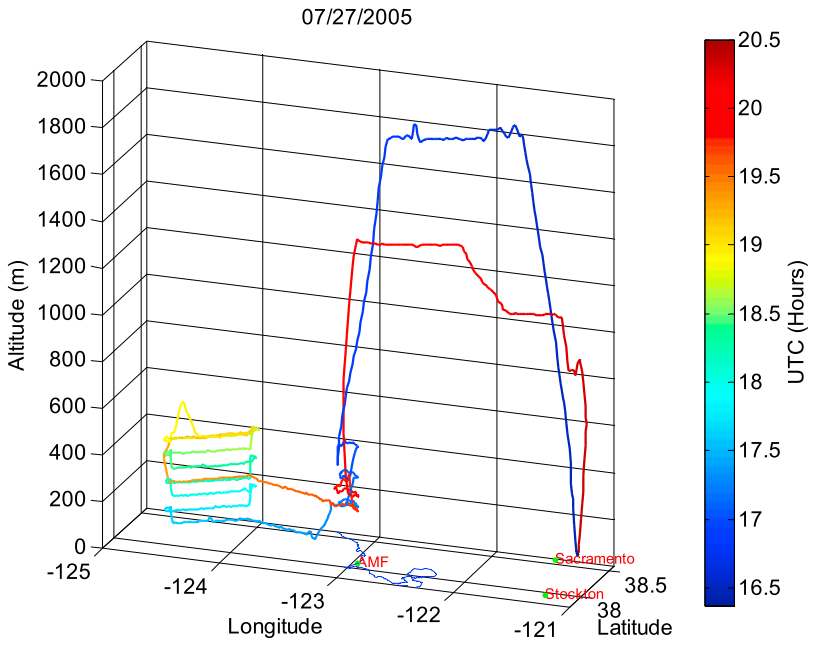

Figure 1. Flight track of G-1 flight on 27 July 2005.

3.1. Vertical Distributions of Cloud Microphysics and Interstitial Aerosol Concentration

[8] Cloud droplet number concentration (N_d) is derived by integrating the droplet size spectrum measured by the CAS for diameters from 1.1 μm to the upper size limit of 54 μm. Averages of N_d are then computed from the 1-s CAS data for each sampling altitude. Figures 2 and 3 show the vertical profiles of average aerosol and cloud microphysical parameters. The horizontal average at each sampling altitude corresponds to about 5 min of data, or a distance of 30 km based on the G-1 cruising speed. The error bars in Figures 2 and 3 indicate one standard deviation of all 1-s data at each altitude, which represent the horizontal variability of the data. Figures 2a–2c show that the average N_d increased with altitude on each of the 3 days. The choice of minimum droplet size (1.1 μm) used for integrating N_d only appreciably affects the average N_d at the lowest sampling level (as indicated by the average droplet size spectra in Figure 9), and the trend of increasing average N_d with altitude is independent of the minimum droplet size. Figures 2d–2f show the average number concentration of particles with diameter between 0.12 and 0.5 μm (N_{PCASP} (D_p < 0.5 μm)) measured by the PCASP. During MASE, total aerosol concentration measured by the PCASP between 0.12 and 0.5 μm often decreased as the G-1 flew into clouds. Figure 4 shows an example on 20 July, in which N_{PCASP} (D_p < 0.5 μm) decreased from ~1200 to ~300 cm^{-3} as the G1 flew a horizontal pass into clouds. Although inlet droplet shattering can produce high concentrations of small droplets (or residue particles after droplet evaporation) [*Weber et al.*, 1998], it appears that the PCASP measurement was not affected by inlet droplet shattering during MASE. This was likely because the heating from the PCASP inlet (the PCASP deicing heater was on during MASE) and sheath flow reduced the size of shattered droplets below the detection limit (~0.12 μm) of the PCASP. It is expected that aerosol particles larger than 0.5 μm in diameter were readily activated into cloud droplets and that cloud droplet diameters exceeded 0.5 μm. Therefore, we expect particles with diameter between 0.12 and 0.5 μm measured by the PCASP inside the clouds were interstitial aerosol particles, and N_{PCASP} (D_p < 0.5 μm) represents the concentration of that subset of the interstitial particles with diameter greater than ~0.12 μm. We estimate that the particle activation diameter for the clouds observed during MASE to be ~0.15 μm by comparing the dry aerosol size spectrum and the average N_d measured inside the cloud (at the sampling altitude of 326 m during the flight on 27 July). As the activation diameter was likely greater than the lower detection limit of the PCASP, most of particles that were not detected by the PCASP (i.e., smaller than 0.12 μm) might be those that always remained unactivated inside the cloud and did not contribute substantially to the variation of interstitial aerosol concentration. We note that N_{PCASP} (D_p < 0.5 μm) may vary when particles move into and out of the measurement size range as RH inside PCASP fluctuates. Given the high RH inside or near cloud, the deicing heater of PCASP would not be able to dry particles completely [*Strapp et al.*, 1992]. As shown in Figures 2 and 6, we mainly examine the variation of N_{PCASP} (D_p < 0.5 μm) during the sampling of cloudy air and clear air pockets inside clouds. The RH inside clouds will be fairly constant, close to 100%. Given the similar ambient RH, we expect both fluctuation of RH inside the PCASP and the corresponding variation of N_{PCASP} (D_p < 0.5 μm) due to particles moving into and out of the measurement size range to be small during the sampling of cloudy air and clear air pockets inside the clouds. Therefore, it is expected that the magnitude of the variation in N_{PCASP} (D_p < 0.5 μm) reflected the variation of total interstitial aerosol concentration. In this study, N_{PCASP} (D_p < 0.5 μm) is therefore used as a surrogate for the interstitial aerosol particle concentration. Figures 2d–2f show that N_{PCASP} (D_p < 0.5 μm) decreased with altitude inside the cloud for the three cases.

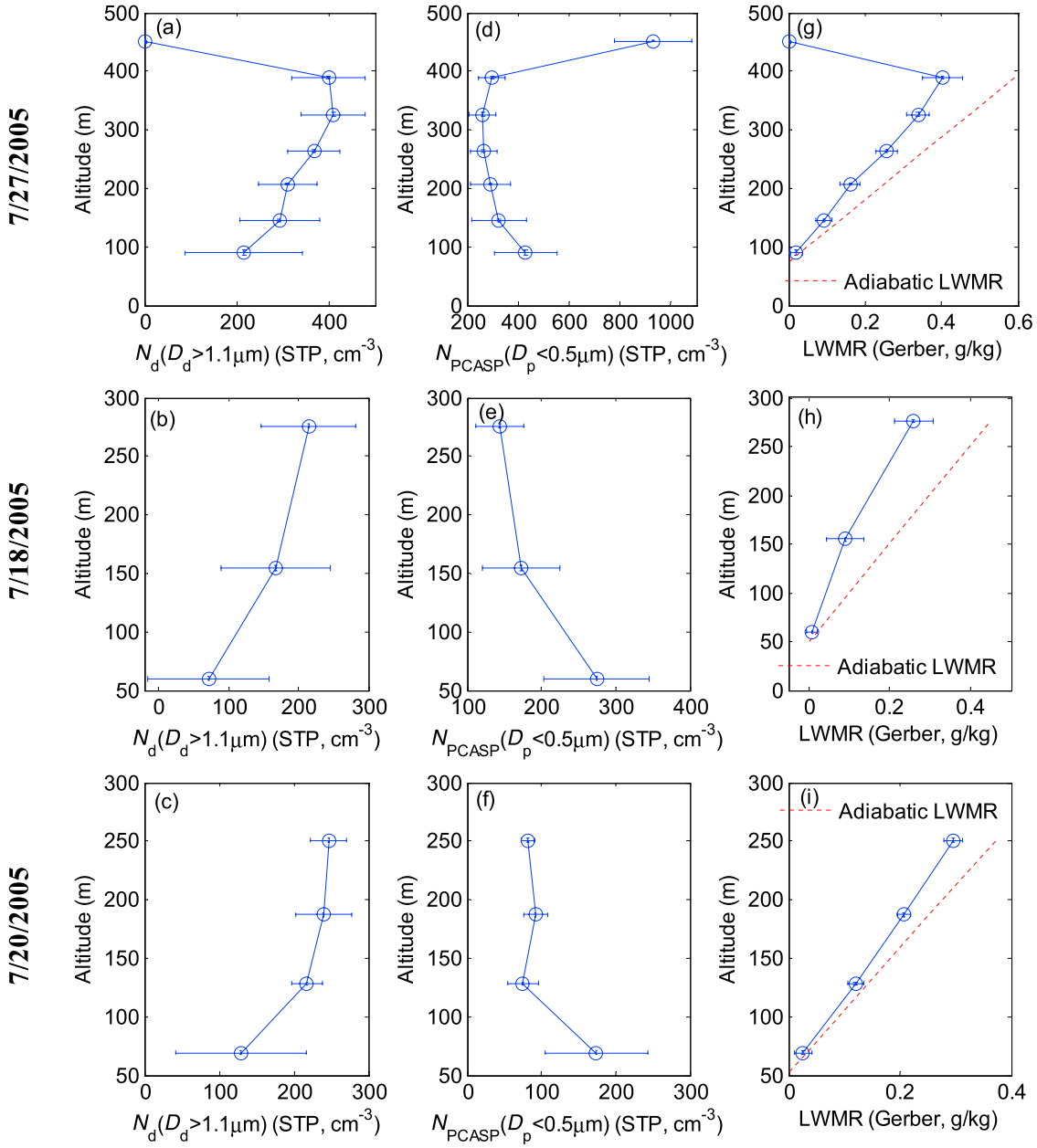

Figure 2. Average and standard deviation calculated from 1 s measurements at each sampling altitude for (a–c) number concentration of droplets between 1.1 and 54 μm in diameter measured by the CAS, (d–f) concentration of particles between 0.12 and 0.5 μm in diameter measured by the PCASP, and (g–i) measured and adiabatic liquid water mixing ratio for the three cases on 27 July 2005 (Figures 2a, 2d, and 2g), 18 July 2005 (Figures 2b, 2e, and 2h), and 20 July 2005 (Figures 2c, 2f, and 2i).

[9] Figures 2g–2i show that the layer-averaged liquid water mixing ratio (LWMR) increased monotonically with altitude, a result of condensational growth as cloud parcels rise. The average cloud base height is determined from the zero intercept of a plot of the horizontal average LWMR against altitude. The adiabatic LWMR is then derived on the basis of the cloud base temperature and pressure [*Brenguier*, 1991]. Figure 2 shows that the measured LWMR was less than the derived adiabatic LWMR for all three cases. As drizzle was minimal in these cases, this suggests the reduction of LWMR below its adiabatic value was the result of entrainment of dry air from above the cloud and subsequent dilution and evaporation of cloud droplets. The liquid water path (LWP) is derived by integrating the vertical profile of measured LWMR from cloud base to the highest sampling level. The LWP on the 3 days was 72%, 69%, and 68% of the adiabatic LWP calculated by integrating the adiabatic LWMR profile.

[10] The standard deviation of droplet diameter (σ_{D_d}) is derived from 1 s measurements of droplet size spectra. The horizontal average of σ_{D_d} exhibited little systematic variation with altitude (Figures 3a–3c). This is in agreement with previous studies, which show that for subadiabatic clouds, σ_{D_d} can be relatively constant over the depth of clouds

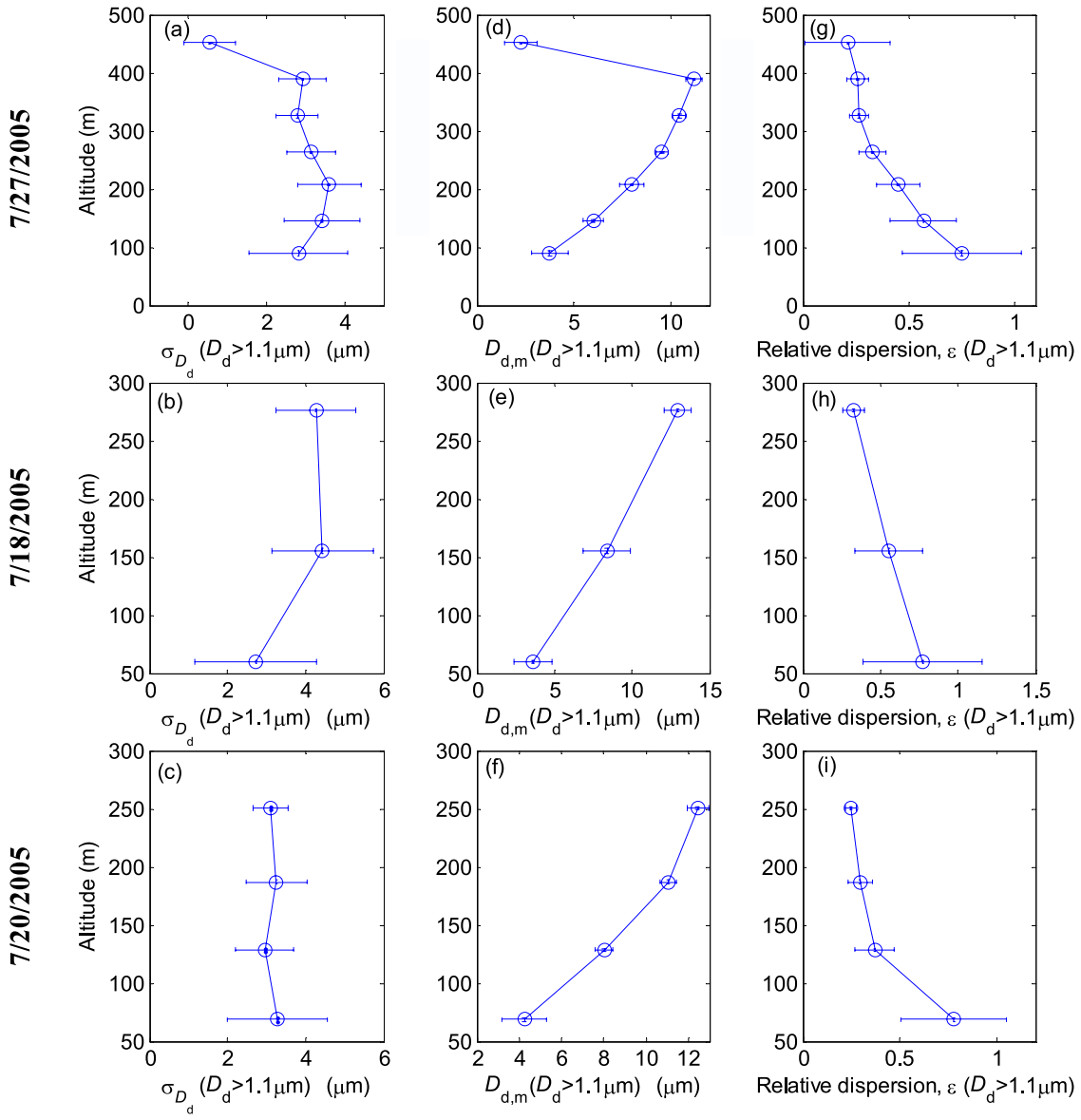

Figure 3. Average and standard deviation calculated from 1 s measurements of droplet size spectra (1.1 to 54 μm) at each sampling altitude for (a–c) standard deviation of droplet diameter, (d–f) mean droplet diameter, and (g–i) relative dispersion for the three cases on 27 July 2005 (Figures 3a, 3d, and 3g), 18 July 2005 (Figures 3b, 3e, and 3h), and 20 July 2005 (Figures 3c, 3f, and 3i).

[*Pawlowska et al.*, 2006; *Lu et al.*, 2007]. As expected, the average of the mean droplet diameter ($D_{d,m}$) increased with altitude as a result of droplet condensational growth (Figures 3d–3f). The relative dispersion, ε, defined as the ratio of σ_{D_d} to $D_{d,m}$, decreased with altitude mainly because of the increase of $D_{d,m}$ (Figures 3g–3i).

[11] Analyses of the measurements suggest that the horizontal variations of cloud microphysics shown in Figures 2 and 3 occurred at relatively small spatial scales instead of the entire sampling distance of ~30 km. Figure 5 shows the horizontal averages and standard deviation of cloud microphysical parameters over distances of 3 km, 8 km, and 36 km. The 3 km and 8 km distances are centered at the middle of the sampling leg (38.12°N and 124.30°W). The vertical profiles are nearly identical for the horizontal averages over different spatial scales. In addition, the horizontal variations over the different spatial scales are very similar. Although it is difficult to determine the scale of the horizontal variation using 1 Hz data (i.e., 100 m spatial resolution), Figure 5 suggests that the horizontal variations occurred at a spatial scale less than 3 km.

3.2. Correlations Among Cloud Microphysical Properties and the Interstitial Aerosol Concentration as a Function of Altitude

[12] Aerosol and cloud microphysical parameters (1 s measurements) are plotted against each other in Figures 6 and 7 at each sampling altitude for the 27 July flight. Correlation coefficients among aerosol and cloud microphysics for all three cases are given in Table 1. Figure 6a and Table 1 show that N_{PCASP} ($D_p < 0.5$ μm), a surrogate for interstitial particle concentration, is negatively correlated

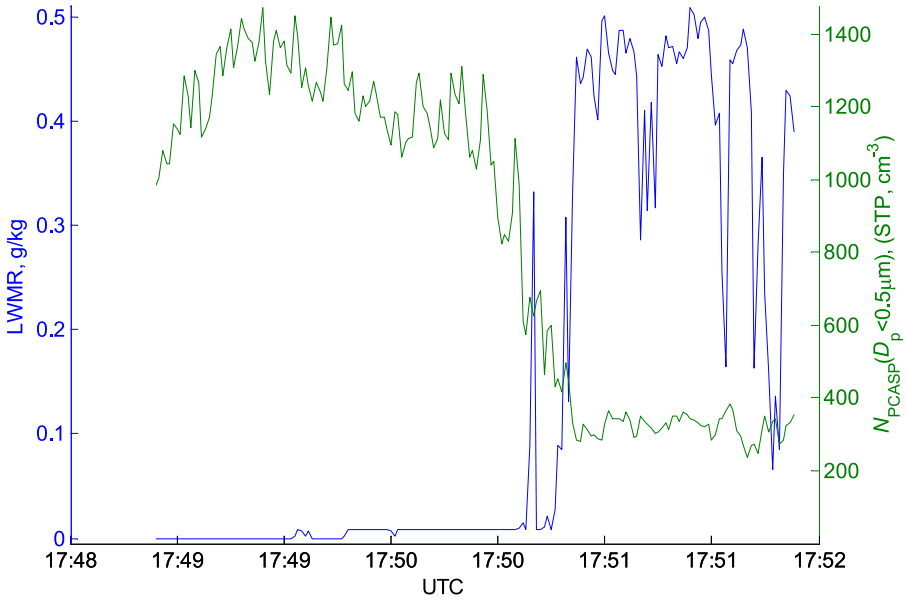

Figure 4. LWMR and N_{PCASP} ($D_p < 0.5$ μm) measured during flight on 20 July 2005. N_{PCASP} ($D_p < 0.5$ μm) decreased from ~1200 to ~300 cm^{-3} as the G1 flew into clouds.

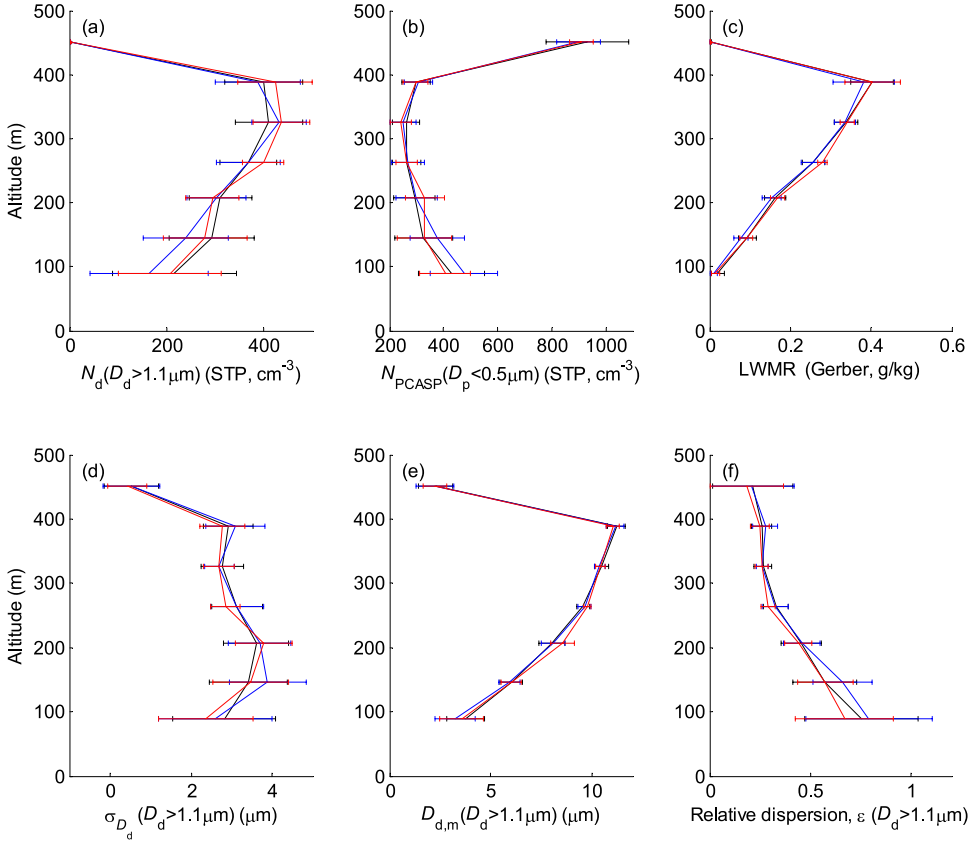

Figure 5. Vertical profiles of the horizontal averages and standard deviations of various cloud microphysical parameters over distances of 3 km (red), 8 km (blue), and 36 km (entire sampling leg, black) for the data on 27 July 2005. The distances of 3 km and 8 km are centered at the middle of the sampling leg (38.12°N and 124.30°W).

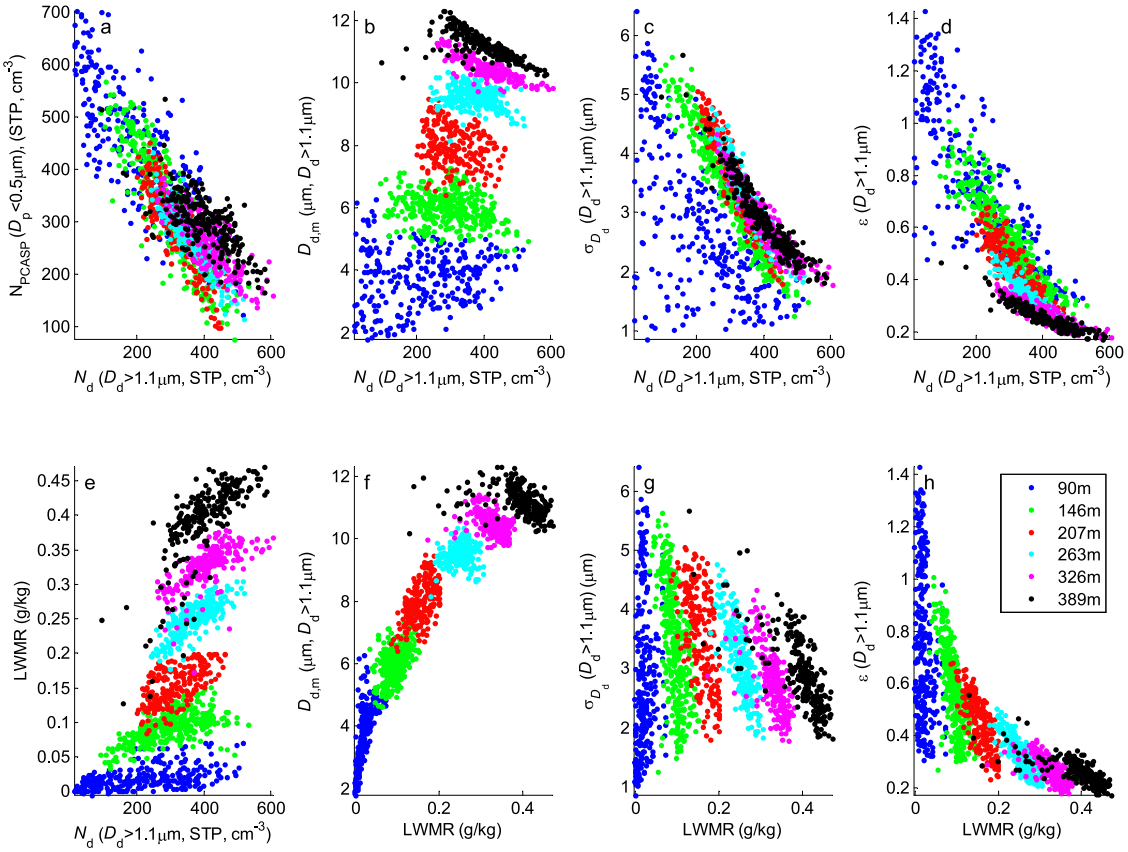

Figure 6. Relationships among interstitial aerosol concentration and cloud microphysical parameters at each sampling altitude for the case on 27 July 2005. The sampling altitude above sea level is listed in the legend.

with N_d. The mean droplet diameter is negatively correlated with N_d at each altitude except at the lower sampling altitudes near the cloud base (Figure 6b and Table 1). Both σ_{D_d} and the relative dispersion (ε) are negatively correlated with N_d at all altitudes, as shown in Figures 6c and 6d and Table 1. These negative correlations are very strong except at the lowest sampling altitudes on 18 and 20 July.

[13] The correlation between $D_{d,m}$ and LWMR also exhibits vertical variations. As drizzle concentration was minimal, the horizontal variation in LWMR likely resulted from mixing processes. $D_{d,m}$ is positively correlated with LWMR at the lower altitudes, but the correlation coefficient gradually decreases with altitude and becomes negative at the highest sampling altitudes inside the cloud. Except for the lowest sampling altitude, σ_{D_d} is negatively correlated with LWMR, and the strength of negative correlation increases with increasing altitude. The negative correlation between ε and LWMR is very strong except at the lowest sampling altitude for all three flights.

[14] To examine the growth of the largest droplets in the clouds, we define $D_{\mathrm{d,\ top\ 5}}$ as,

$$\int_{D_{\mathrm{d,top5}}}^{\infty} n(D_d)dD_d = 5\ \mathrm{cm}^{-3} \qquad (1)$$

where $D_{\mathrm{d,\ top\ 5}}$ represents the minimum diameter of the largest 5 droplets per 1 cm^3 of cloud air. Similarly, $D_{\mathrm{d,\ top\ 10}}$ is defined as the minimum diameter of the largest 10 droplets within 1 cm^3 cloud air. During MASE, the concentration of droplets detected in the largest size bin of the CAS (41–54 μm) was always less than 5 cm^{-3}, and $D_{\mathrm{d,\ top\ 5}}$ and $D_{\mathrm{d,\ top\ 10}}$ are calculated from the measured droplet size spectra using equation (1). We note that $D_{\mathrm{d,\ top\ 5}}$ and $D_{\mathrm{d,\ top\ 10}}$ can be derived only for measurements with total droplet number concentration greater than 5 and 10 cm^{-3}, which represent the majority of in-cloud measurements. It is worth pointing out that, unlike $D_{d,m}$, neither $D_{\mathrm{d,\ top\ 5}}$ nor $D_{\mathrm{d,\ top\ 10}}$ is influenced by the formation or evaporation of new (small) droplets at the lower range of the droplet spectrum, and thus are more direct measures of the largest droplets in a cloud parcel. Figure 7 shows that both $D_{\mathrm{d,\ top\ 5}}$ and $D_{\mathrm{d,\ top\ 10}}$ increase as LWMR decreases except at the lowest sampling altitudes near cloud base, suggesting that larger droplets were produced in cloud parcels with lower LWMR.

4. Discussion

[15] This section considers explanations for the observed microphysical behavior. Mixing processes can be interpreted in terms of various entrainment models or a stratocumulus circulation model [*Betts*, 1978, 1983; *Schubert et al.*, 1979] described in section 4.1. On the basis of this stratocumulus circulation model, a mixing process between cloud parcels is proposed to explain the observed vertical and horizontal variations of N_d and interstitial aerosol

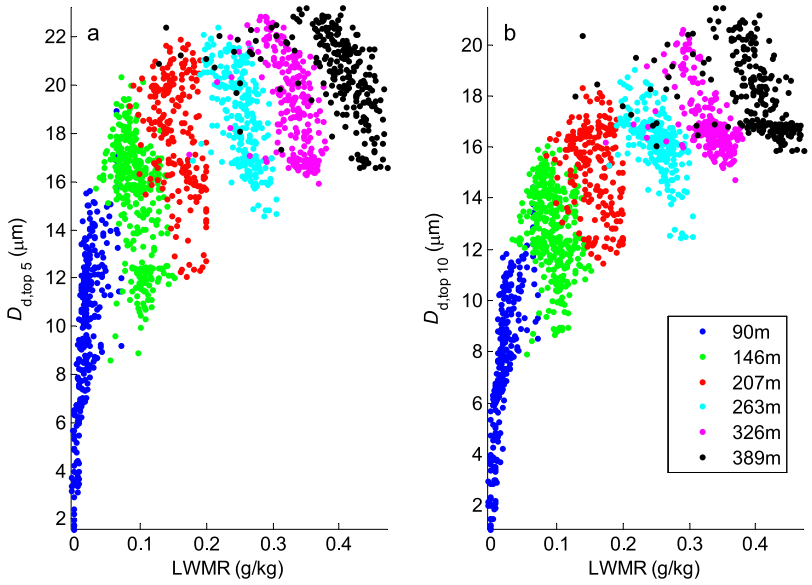

Figure 7. (a) $D_{d,\ top\ 5}$ and (b) $D_{d,\ top\ 10}$ as a function of LWMR at each sampling altitude for the case on 27 July 2005. The sampling altitude above sea level is listed in the legend.

concentration (section 4.2), and the vertical variations of correlations among cloud microphysical parameters (sections 4.3 and 4.4). In section 4.5, three conceptual models of entrainment mixing, including homogeneous mixing, inhomogeneous mixing, and entity type entrainment mixing, are considered with regard to implications in terms of cloud microphysics.

4.1. Stratocumulus Circulation Model

[16] Convection in stratocumulus-topped boundary layers can be described as circulations of air parcels in the boundary layer [*Betts*, 1978, 1983; *Schubert et al.*, 1979]. Air parcels receive water vapor from the ocean surface and their water content is reduced by mixing with entrained dry air from above cloud top. As the drizzle concentration was very low in the cases studied here, the effect of drizzle on cloud liquid water is neglected. The red lines in Figure 8 show an idealized LWMR of a circulating cloud parcel as a function of altitude (the same as *Schubert et al.* [1979, Figure 15]). For the ascending branch of the circulation, a parcel first rises from the ocean surface (point A in Figure 8). The parcel LWMR remains zero until the parcel rises to its lifting condensation level (LCL), indicated by point B in Figure 8. As the parcel continues to rise above its LCL (point B), it follows a wet adiabat and its LWMR increases with altitude following the liquid water increase rate of an adiabatic parcel. At the cloud top (point C), the cloud parcel mixes with entrained clear air, which reduces the LWMR of the parcel (from point C to D). Evaporative and radiative cooling at the cloud top overwhelm the warming because of the mixing with warmer air entrained from above the cloud, and the cloud parcel starts to descend along a wet adiabat with a lower temperature and LWMR [*Schubert et al.*, 1979]. As the LWMR is lower in the descending branch of the circulation, the wet adiabatic descent cannot continue to the same LCL (point B). Instead, it terminates at a higher altitude (indicated by point E) where the LWMR reaches zero, and leads to a higher Local Cloud Base Height (LCBH). Further descent of the parcel below point E follows a dry adiabat (i.e., LWMR remains

Table 1. Correlation Coefficients Between Aerosol and Cloud Microphysics Calculated From 1 s Data as a Function of Sampling Altitude

Flight Date	Altitude (m)	γ [N_{PCASP}, N_d]	γ [$D_{d,m}$, N_d]	γ [σ_{D_p}, N_d]	γ [ε, N_d]	γ [LWMR, N_d]	γ [$D_{d,m}$, LWMR]	γ [σ_{D_p}, LWMR]	γ [ε, LWMR]	γ [$D_{d,top5}$, LWMR]	γ [$D_{d,top10}$,LWMR]
27 Jul 2005	389	−0.71	−0.71	−0.94	−0.92	0.74	−0.36	−0.74	−0.76	−0.43	−0.41
27 Jul 2005	326	−0.81	−0.83	−0.93	−0.90	0.67	−0.35	−0.67	−0.69	−0.51	−0.55
27 Jul 2005	263	−0.88	−0.32	−0.96	−0.93	0.79	0.18	−0.78	−0.84	−0.59	−0.56
27 Jul 2005	207	−0.87	−0.23	−0.95	−0.89	0.62	0.55	−0.56	−0.78	−0.33	−0.30
27 Jul 2005	146	−0.90	−0.26	−0.96	−0.92	0.63	0.49	−0.58	−0.74	−0.37	−0.23
27 Jul 2005	90	−0.81	0.15	−0.65	−0.84	0.48	0.68	0.11	−0.27	0.68	0.77
18 Jul 2005	276	−0.77	−0.79	−0.94	−0.88	0.85	−0.41	−0.83	−0.86	−0.62	−0.64
18 Jul 2005	155	−0.85	0.36	−0.84	−0.85	0.84	0.68	−0.60	−0.83	0.58	0.64
18 Jul 2005	60	−0.89	0.63	−0.20	−0.53	0.79	0.71	0.02	−0.36	0.77	0.74
20 Jul 2005	251	−0.50	−0.97	−0.89	−0.83	0.73	−0.71	−0.80	−0.79	−0.78	−0.76
20 Jul 2005	187	−0.21	−0.85	−0.93	−0.90	0.69	−0.39	−0.58	−0.60	−0.50	−0.49
20 Jul 2005	129	−0.59	0.15	−0.88	−0.86	0.54	0.80	−0.55	−0.64	−0.38	−0.30
20 Jul 2005	69	−0.93	0.56	−0.30	−0.73	0.72	0.84	0.20	−0.36	0.91	0.91

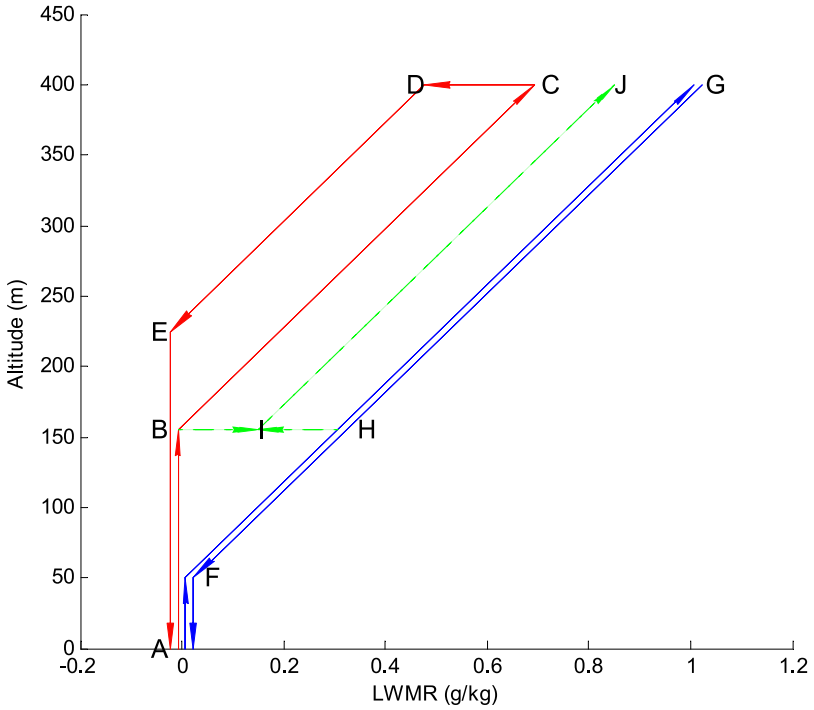

Figure 8. LWMR as a function of altitude for circulating cloud parcels and mixture of cloud parcels with different TWMR. The LWMR of circulating parcels is represented by the red lines [*Schubert et al.*, 1979].

zero). When arriving at the ocean surface, the descending parcel receives water vapor from the ocean surface and begins another circulation.

[17] In ambient clouds, cloud parcels are expected to exhibit a range of values of total water mixing ratio (TWMR), as the entrainment mixing and transfer of water vapor from the ocean surface are not equal in all cloud parcels. As a result, cloud parcels follow different circulation paths on the LWMR-altitude diagram (Figure 8). For example, cloud parcels that are not affected by entrainment mixing have the highest TWMR and LWMR. To the first order, their ascending and descending branches follow the same path but opposite directions on the LWMR-altitude diagram (shown as blue lines in Figure 8). These parcels also have the lowest LCL (point F in Figure 8). Other cloud parcels will have lower TWMR due to the mixing with dry air entrained from above cloud top and thus have higher LCL. We note that cloud parcels may lose their identity by mixing with other cloud parcels. The mixtures then follow new circulation paths on the LWMR-altitude diagram before mixing with yet other cloud parcels. Previous observations found that in stratocumulus clouds, the downdraft regions are often narrow surrounding broader updraft regions [*Caughey et al.*, 1982; *Nicholls*, 1989; *Gerber et al.*, 2005]. *Nicholls* [1989] showed that downdrafts occupy narrow regions ($\sim$0.1–0.15h wide, h being the mean mixed layer depth) around the periphery of larger, regular ($\sim$0.5$\sim$0.75h) updraft regions in stratocumulus clouds. Therefore, we expect measurements at a constant altitude may be dominated by sampling of ascending cloud parcels.

4.2. Vertical Variations of N_d and Interstitial Aerosol Concentration

[18] It is generally considered that the maximum supersaturation within a rising cloud parcel is reached near the cloud base. This conceptual model suggests that except for the lowest sampling level, which could be below the altitude where maximum supersaturation is reached, N_d measured at other sampling levels inside the cloud would be independent of altitude, instead of increasing with altitude as observed during MASE and in previous field measurements [*Duynkerke et al.*, 1995, Figure 7a].

[19] There are several potential explanations for the observed increase in N_d with altitude. During MASE, a thin layer of aerosol with higher number concentration was often observed just above the cloud. Entrainment of above-cloud air with higher aerosol concentrations could lead to increases in CCN concentration (N_{CCN}) and possibly, the increased N_d near cloud top. However, the aerosol within this thin layer was dominated by organic species and had higher concentrations of both CCN and particles that were too small or not soluble enough to activate at the supersaturation of the cloud [*Wang et al.*, 2008]. If the increase in N_d was mainly due to increasing aerosol concentration resulting from entrainment of the layer, we would expect that both interstitial aerosol concentration and N_d would increase with increasing altitude, instead of the opposite trends of N_{PCASP} (D_p < 0.5 μm) and N_d observed for the cases (Figure 2). We note that the entrained air with higher aerosol concentrations does not always stay at the cloud top. The circulation of parcels within the boundary layer tends to homogenize the vertical distribution of aerosol. In addition,

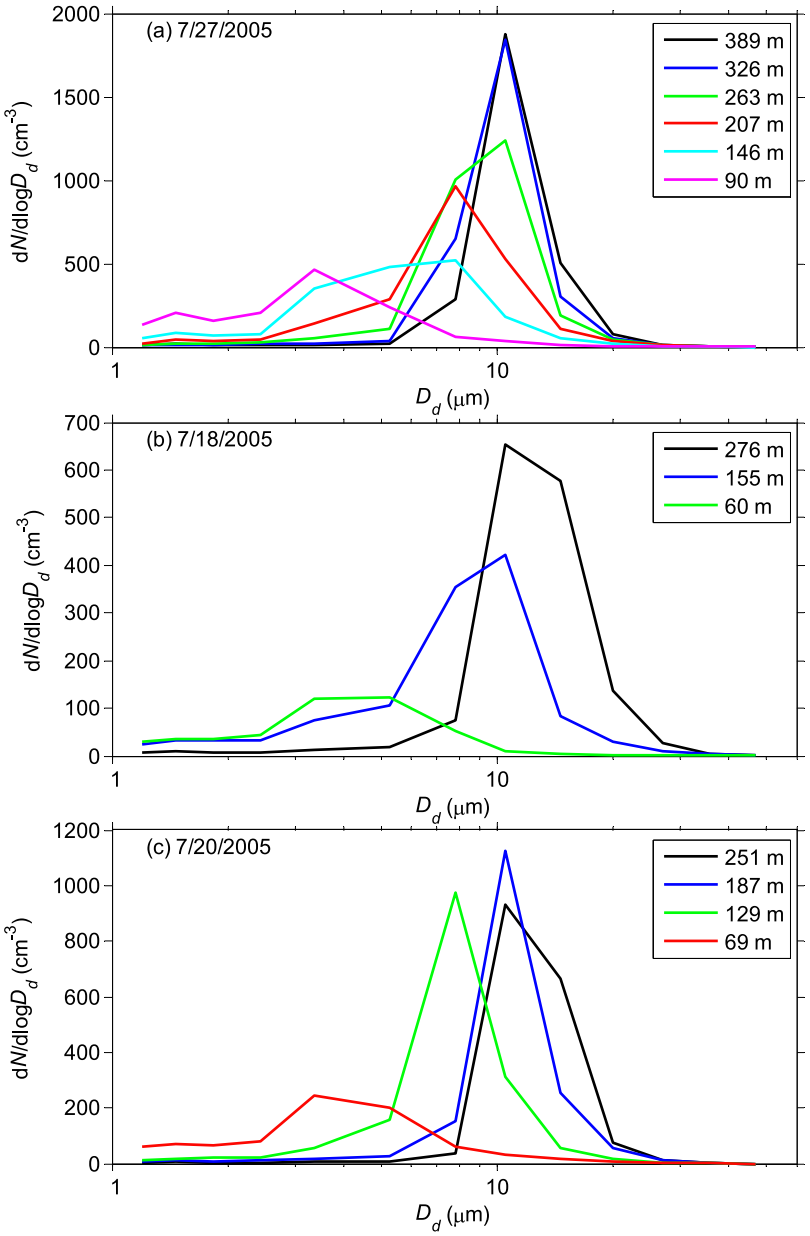

Figure 9. Average droplet size spectrum at each sampling altitude for the three cases on (a) 27 July 2005, (b) 18 July 2005, and (c) 20 July 2005.

N_{PCASP} (D_p < 0.5 μm) measured in the layer above cloud was about 900 cm^{-3}, only 40% higher than that measured below the cloud. As a result, entrainment of the layer likely did not lead to a substantial vertical gradient of the total aerosol concentration, and was unlikely the main reason for the observed significant increase of N_d with increasing altitude. Another possible mechanism to produce lower N_d at lower altitude in cloud is the scavenging of cloud droplets by drizzle. Drizzle often forms near the top of the cloud, and as drizzle drops fall, they may scavenge smaller droplets through collision-coalescence. However, as interstitial aerosol concentration is not affected by drizzle, such a mechanism also fails to explain the opposite trend of the decreasing interstitial aerosol concentration with increasing altitude. In addition, the drizzle concentration in the three cases was very low.

[20] The increase of N_d with altitude could also be due to the growth of small droplets initially below the detection threshold into the CAS measurement size range as altitude increases. Figure 9 shows the horizontal average droplet spectrum measured at each sampling altitude for the three cases. At the lowest sampling levels, the size spectra indicate some small droplets below the CAS threshold, which likely contributed to the increases in N_d from the lowest sampling level to the next level above. This is the case especially for the flight on 27 July. However, at higher sampling altitudes, the size spectra show peak diameter significantly greater than the CAS threshold and negligible droplet concentration near the threshold, suggesting that most of the droplets had grown above the lower size detection limit. While the growth of initially undetected small droplets may explain the increase of N_d at lower

altitude, it was unlikely the main reason for the observed vertical N_d gradient at higher sampling altitudes shown in Figure 2.

[21] A mechanism for the observed vertical gradient in N_d is suggested by the stratocumulus circulation model described above. It is expected that the inhomogeneity of entrainment mixing and the humidification of cloud parcels by the ocean surface generate air parcels with a range of TWMR values, which in turn, leads to variations in LCBH as these air parcels ascend. This variability is supported by the measurements at the lowest altitude, which show that both clear air (i.e., measurements with LWMR = 0 as shown in Figure 6f) and cloudy air existed at the same altitude. It is worth noting that the 1 s measurements on board G-1 correspond to a spatial resolution of 100 m. Measurements that appeared as cloudy air might include clear air pockets with spatial scales less than 100 m. Given the variations in LCBH, measurements at a lower altitude likely include more sampling of clear air below LCBH. As a result, the average N_d at a lower altitude can be lower than that measured at a higher altitude, where less sampling of clear air (below LCBH) is expected and droplet sizes are also more likely to be greater than the lower detection threshold of CAS. This would lead to an apparent increase of the average N_d with altitude (Figures 2a–2c). Such a picture is also consistent with the decreasing trend of interstitial aerosol concentration with increasing altitude (Figures 2d–2f) because less sampling of clear air at higher altitudes leads to a lower N_{PCASP} ($D_p < 0.5$ μm). The above mechanism can also explain the negative correlation between N_{PCASP} ($D_p < 0.5$ μm) and N_d at each altitude shown in Figure 6a and Table 1.

4.3. Correlation Between N_d and $D_{d,m}$, σ_{D_d}, and ε

[22] During MASE, $D_{d,m}$ was negatively correlated with N_d except at the lowest sampling altitudes. A negative correlation between $D_{d,m}$ and N_d was also observed in previous studies [e.g., *Curry*, 1986; *Hudson and Svensson*, 1995; *Hudson and Li*, 1995; *Brenguier et al.*, 2000; *Pawlowska and Brenguier*, 2000]. In those studies, the variation in N_d was attributed mainly to the variation in updraft velocity (w) at cloud base rather than the variation in CCN concentration below cloud. A higher cloud base w leads to a higher maximum supersaturation, and consequently a higher N_d. Because of the competition for water vapor among more numerous droplets, the higher N_d leads to a smaller droplet size. As a result, the variation of N_d due to the variation of cloud base w should be negatively correlated to $D_{d,m}$.

[23] The above explanation for the correlation between $D_{d,m}$ and N_d assumes adiabatic cloud parcels, whereas the actual cloud parcels sampled exhibited a range of adiabaticity and TWMR. Compared to N_d, adiabatic LWMR at a given altitude is almost independent of w [e.g., *Twomey*, 1977], and the observed variation in LWMR can be taken to reflect the horizontal variation of adiabaticity or the LCBH. Figure 2 shows that the horizontal variations of N_d are much greater than those of LWMR. With the G1 cruising speed of 100 m s^{-1}, the CAS sampling volume for 1 s measurements is about 14 cm^3. At the typical droplet number concentration of 200–400 cm^{-3}, the uncertainty in N_d due to counting statistics is less than 2%. Therefore, the large variation of N_d observed during sampling at constant altitudes was mainly due to horizontal variation instead of counting statistics of the CAS. Because the mean droplet diameter of a cloud parcel is mainly influenced by its N_d and LWMR, the much greater horizontal variations of N_d compared to those of LWMR suggest that the variation in $D_{d,m}$ at a constant sampling altitude was mainly due to the variation in N_d, which is attributed mainly to the variation of cloud base w. This may explain why N_d is generally negatively correlated with $D_{d,m}$ in the body of the cloud despite the fact that the cloud parcels had a range of cloud base height.

[24] At flight levels close to cloud base, N_d is instead positively correlated with $D_{d,m}$. The positive correlation is very weak for the flight on 27 July. Parcels with lower LWMR generally have smaller droplets, which may be below the threshold of the CAS at the lowest sampling level. As a result, these parcels with lower LWMR exhibit both lower N_d and $D_{d,m}$, which lead to a positive correlation. This positive correlation could also be a consequence of the low time resolution of the CAS measurement (1Hz) described as follows. It is expected that at lower altitudes, measurements in the area with low TWMR are more likely to include both clear air parcels (below its LCBH) and cloud parcels with low LWMR and therefore small $D_{d,m}$, which, lumped together into one CAS measurement volume, exhibit both a smaller $D_{d,m}$ and a lower N_d. In contrast, measurements in the high TWMR area will generally include cloud parcels with larger $D_{d,m}$ and a smaller fraction of clear air. This can also potentially explain the positive correlations between $D_{d,m}$ and N_d observed at lower altitudes (Table 1).

[25] Figure 6c and Table 1 show σ_{D_d} negatively correlated with N_d, also in agreement with previous studies [*Hudson and Svensson*, 1995; *Yum and Hudson*, 2005]. *Hudson and Svensson* [1995] explained the negative correlation between σ_{D_d} and N_d as follows. First, low N_d is often associated with low w, which produces a broad distribution and high σ_{D_d} [*Srivastava*, 1991; *Yum and Hudson*, 2005]. Second, as discussed earlier, variation in cloud base w leads to variation in $D_{d,m}$ at the same altitude. Whereas an individual parcel may have a narrow size spectrum, it is expected that σ_{D_d} increases when parcels with different cloud base w mix together or simply are lumped together into a measurement volume. High N_d often corresponds to low σ_{D_d}, which is consistent with parcels that have high cloud base w. Parcels with high N_d are less likely to be mixtures with different cloud base w because mixing generally reduces N_d. Despite the inverse relationship between $D_{d,m}$ and N_d, the rapid increase of σ_{D_d} with decreasing N_d leads to negative correlation between the relative dispersion (ε) and N_d as shown in Figure 6d and Table 1.

4.4. Circulation Mixing and Correlation Between LWMR and Other Cloud Microphysical Parameters

[26] Figure 6f and Table 1 show that the correlation between $D_{d,m}$ and LWMR varies with altitude within the clouds. For the 27 July 2005 case, at the lower four altitudes of 90, 146, 207, and 263 m, $D_{d,m}$ is positively correlated with LWMR. The correlation coefficient decreases with altitude and becomes negative at the highest two altitudes (326 and 389 m). As discussed earlier, ascending cloud

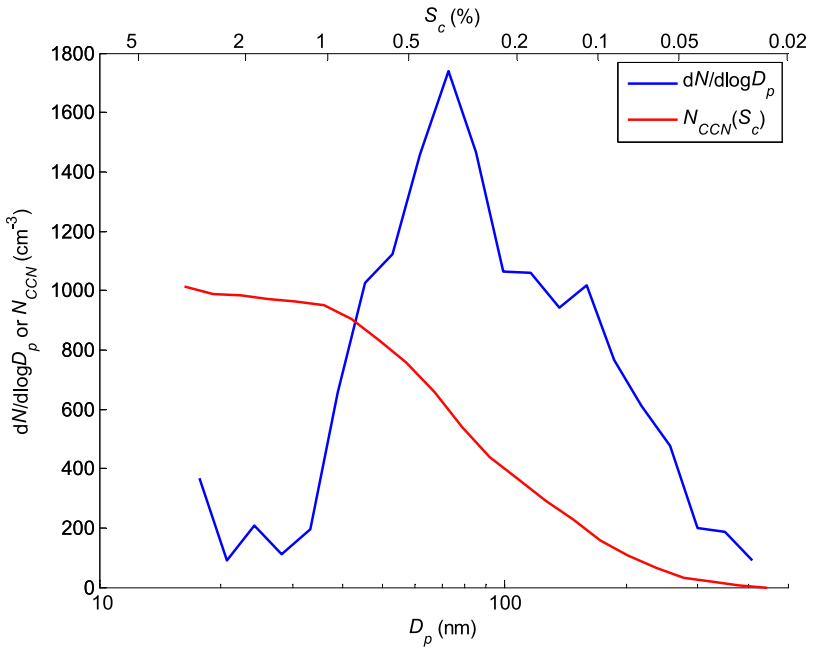

Figure 10. Aerosol size distribution and CCN spectrum used as input for cloud parcel model, where D_p is the dry particle size and S_c is the critical supersaturation.

parcels likely exhibit a range of TWMR, resulting in a range of local LCLs. A cloud parcel can also lose its identity by mixing with other cloud parcels to form a mixture with new TWMR and LWMR. An example of such mixing is illustrated in Figure 8, which shows the evolution of LWMR after a parcel with lowest LCL (i.e., highest TWMR, point H) mixes with another parcel at its higher LCL (i.e., lower TWMR, point B). The two parcels are referred to as the LLCL parcel and HLCL parcel. At its LCL, the HLCL parcel is saturated (100% RH) but free of cloud droplets. At the same altitude, cloud droplets have already grown in the LLCL parcel as it has lower LCL (point F) and higher LWMR. Owing to the dilution by the saturated but droplet-free HLCL parcel, the mixture of the two parcels has lower LWMR (point I on Figure 8) than the original LLCL parcel, and during its subsequent ascent, the LWMR of this mixed parcel will follow the path from point I to point J shown as green lines in Figure 8.

[27] To examine this mixing process, the evolution of cloud microphysics during ascent was simulated using a cloud parcel model [*Robinson*, 1984] for the LLCL parcel and the mixtures. The CCN spectrum used as input was derived from the aerosol size distribution measured near the cloud base by a scanning mobility particle sizer and the average aerosol composition measured by an Aerodyne Aerosol Mass Spectrometer assuming internal mixing [*Wang et al.*, 2008]. The CCN spectrum and aerosol size distribution are shown in Figure 10. In the simulations, the LLCL parcel with LCL of 50 m was allowed to rise 100 m above its LCL and then was mixed with another parcel that had a LCL of 150 m. Simulations were carried out for the volume mixing ratios of 70:30, 50:50, and 30:70. An updraft velocity of 20 cm s^{-1}, which is within the range measured near cloud base during MASE, was used [*Lu et al.*, 2007]. A simulation using a different updraft velocity 50 cm s^{-1} shows the same main features after the mixing. Figure 11c shows that the mixing first dilutes the LLCL parcel and leads to a reduction in N_d. The decreased N_d results in a smaller sink for water vapor. As a result, a local maximum supersaturation (S) is formed rapidly during the subsequent ascent of the mixture. Figure 11b shows that the local maximum S after the mixing is considerably lower than the maximum supersaturation near the cloud base. Therefore only a small percentage of particles (i.e., those particles that have low critical supersaturation) from the HLCL parcel is activated. This leads to only a slight increase in N_d of the mixture, which is still substantially lower than that of the LLCL parcel in the absence of mixing.

[28] Because of the formation of the new droplets after mixing, $D_{d,m}$ of the mixture (with lower LWMR) is initially smaller than that of the LLCL parcel (with higher LWMR). This could contribute to the positive correlation between $D_{d,m}$ and LWMR at lower altitudes. However, as the surface area of the newly formed droplets in the mixture is smaller than that of the large droplets from the LLCL parcel, water vapor preferentially condenses on the large droplets. Consequently, a disproportionate share of water vapor condenses on the large droplets, which grow to greater sizes than those in the unmixed LLCL parcel. It is expected that this enhanced growth of large droplets will be most pronounced when parcels with very different LCLs are mixed. For the three volume mixing ratios simulated, the enhanced growth of large droplets eventually leads to higher $D_{d,m}$ of the mixture than that of the LLCL parcel, as shown in Figure 11d. This can explain the transition of the correlation coefficient between $D_{d,m}$ and LWMR from positive at lower altitudes to negative at the cloud top. The mixing process described above is referred to here as "circulation mixing." The enhanced growth of large droplets due to circulation mixing is also evident in Figure 11f, which shows that for the three volume mixing ratios simulated, $D_{\max}$(the diameter

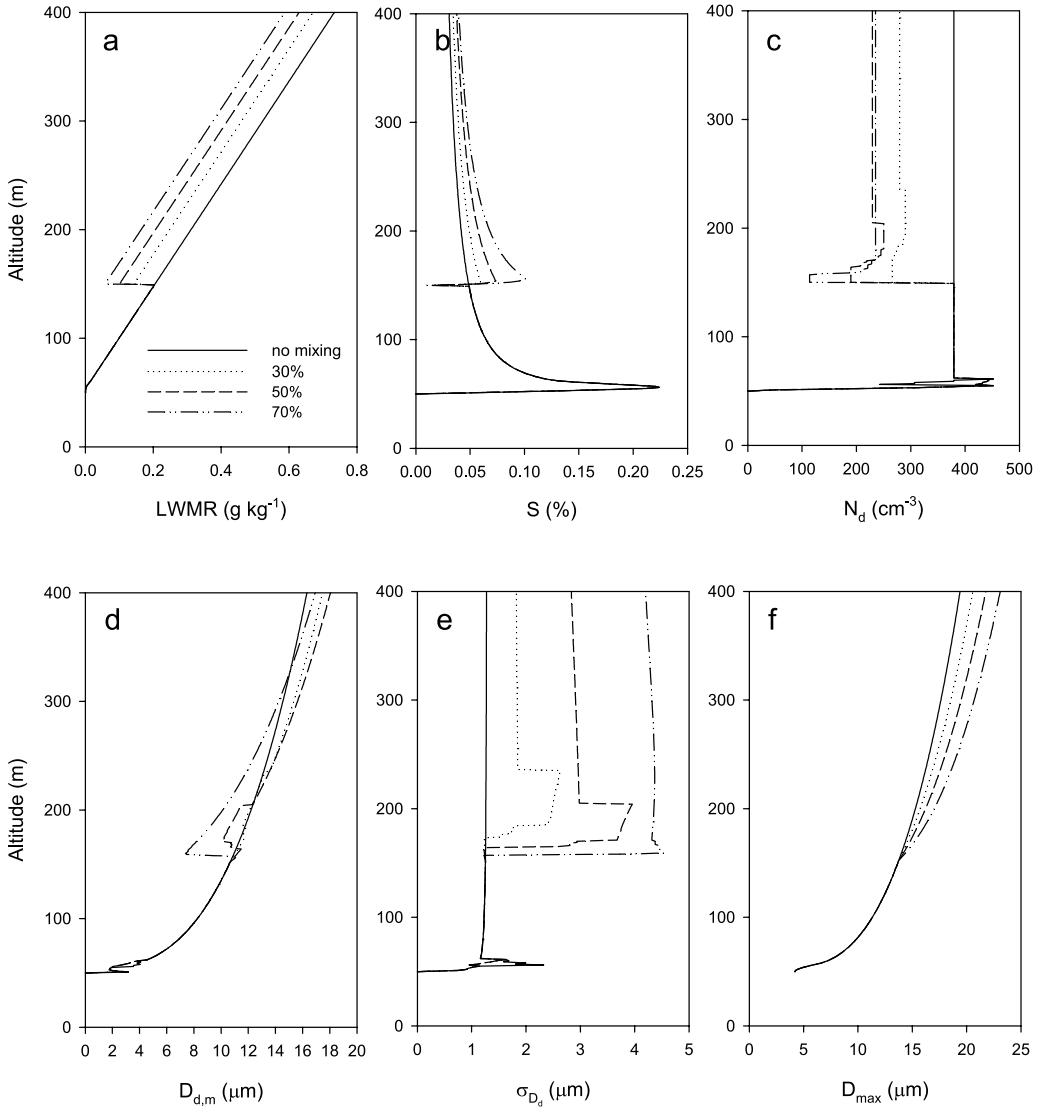

Figure 11. Modeled evolutions of (a) liquid water mixing ratio, (b) supersaturation, (c) droplet number concentration, (d) mean droplet diameter, (e) standard deviation of droplet diameter, and (f) the diameter of the largest droplet size bin for a LLCL cloud parcel and mixtures of the LLCL and HLCL cloud parcels with volume mixing ratio of 70:30, 50:50, and 30:70. The LLCL cloud parcel has a LCL of 50 m and is mixed with the HLCL parcel at its LCL of 150 m.

of the largest droplet size bin) of the mixture is substantially larger than that of the unmixed LLCL parcel. The larger $D_{\max}$ for the diluted mixture with lower LWMR is consistent with the negative correlations between LWMR and $D_{\mathrm{d,\ top\ 5}}$ and $D_{\mathrm{d,\ top\ 10}}$ shown in Figure 7. Prior to circulation mixing, cloud parcels with higher LWMR generally have larger droplet sizes than those with lower LWMR at the same altitude, which could also contribute to the positive correlations between LWMR and $D_{d,m}$, $D_{\mathrm{d,\ top\ 5}}$, and $D_{\mathrm{d,\ top\ 10}}$ at lower altitudes shown in Figure 6f and Table 1. If the majority of HLCL cloud parcels (i.e., with low LWMR) reach the cloud top without mixing with the LLCL parcels, we expect that $D_{d,m}$, $D_{\mathrm{d,\ top\ 5}}$, and $D_{\mathrm{d,\ top\ 10}}$ would be positively correlated with LWMR, even at cloud top. The negative correlations suggest that the majority of HLCL cloud parcels with low LWMR were mixed before reaching the cloud top.

[29] In circulation mixing, the dilution by HLCL parcels reduces both LWMR and N_d, of the mixture (Figures 11a and 11c), which contributes to a positive correlation between LWMR and N_d, as shown in Figure 6e. In addition, when cloud parcel and clear air (parcel below its LCBH) are simply lumped together into a single measurement volume, the measurement will show both a lower LWMR and a lower N_d. This potential sampling artifact could also contribute to the positive correlation between LWMR and N_d. Figure 11e shows that for all volume mixing ratios simulated, the mixtures have much higher σ_{D_d} than the unmixed LLCL parcel. This is due to the formation of smaller droplets and enhanced growth of large droplets, both of which broaden the droplet spectrum and increase σ_{D_d}. As a result, we expect σ_{D_d} to be negatively correlated with LWMR as shown in Figure 6g. In addition, cloud parcels at the same altitude but with different LWMRs generally

have different droplet sizes. Therefore, even without circulation mixing, broadening of the measured spectrum and reduced LWMR are expected if parcels with different LWMRs are simply measured together. This sampling artifact could also lead to high σ_{D_d} for measurements exhibiting overall low LWMR (Figure 6g). The rapid increase of σ_{D_d} with decreasing LWMR leads to negative correlations between ε and LWMR (Figure 6h and Table 1) despite the negative correlation between $D_{d,m}$ and LWMR at the cloud top.

[30] The dilution of LLCL cloud parcels by HCLC parcels can occur over a range of altitudes in addition to the LCL (point B in Figure 8). Mixing of the two parcels at other altitudes near the LCL of the HLCL parcel (point B) also leads to enhanced growth of large droplets through the same mechanism described earlier. For example, at an altitude just above its LCL, the HLCL parcel has smaller droplets compared to the LLCL parcel. In the mixture of the two parcels, the small droplets originating from the HLCL parcel have smaller surface area, and a larger share of water vapor condenses on the fewer large droplets originating from the LLCL parcel. This also leads to enhanced growth of large droplets compared to those in unmixed LLCL parcels. The mixture can also continue to mix with other HLCL cloud parcels (with higher LCL and lower LWMR) during its ascent to the cloud top. This subsequent mixing further reduces the LWMR of the mixture, and further dilutes and enhances the growth of the large droplets. Whereas the example shown in Figure 8 involves a parcel with the lowest LCL (i.e., parcel not affected by entrainment mixing), for the same reason, enhanced growth of large droplets is expected when any cloud parcel is diluted by another parcel with lower TWMR at or near its higher LCL.

4.5. Cloud Top Entrainment Mixing

[31] At the cloud top, mixing between cloudy parcels and entrained clear air from above cloud reduces the LWMR of the cloud parcel. Two conceptual mixing models have been advanced on the basis of analysis of the time scales for the droplet evaporation and complete homogenization of the clear air and cloud parcel mixture. In the inhomogeneous mixing model, droplets in part of a cloud parcel exposed to subsaturated clear air will completely evaporate within the clear air, which is progressively moistened until reaching equilibrium supersaturation [*Baker et al.*, 1980]. Therefore, a subset of droplets is completely evaporated while the sizes of the rest of the droplets in the parcel remain unchanged. As a result, the shape of the droplet size spectrum is maintained following the inhomogeneous mixing. Some previous studies [e.g., *Pawlowska and Brenguier*, 2000; *Burnet and Brenguier*, 2007; *Haman et al.*, 2007] show significant variation of N_d at the top of stratocumulus, while the droplet mean volume diameter appears almost constant, which is attributed to inhomogeneous mixing.

[32] In the homogeneous mixing model, in contrast, the clear and cloudy air mix homogeneously, then evaporation occurs simultaneously from all droplets until saturation is achieved uniformly in the mixed volume [*Warner*, 1973; *Mason and Jonas*, 1974]. Therefore, homogeneous mixing leads to immediate reductions in both droplet size and LWMR, which translate into a positive correlation between $D_{d,m}$ and LWMR. Figure 6f may show some trace of this behavior: at the highest altitude (389 m) sampled in the cloud, a small fraction of the data are scattered at much lower LWMR (less than 0.35 g kg^{-1}) than the majority of the measurements and they did show a positive correlation (0.3 for $D_{d,m}$ versus LWMR). Possibly these were cloud parcels recently affected by entrainment and homogeneous mixing near cloud top. These parcels have reduced LWMR and $D_{d,m}$, and therefore the correlation between $D_{d,m}$ and LWMR resulting from circulation mixing is weakened. Although it is somewhat arbitrary, removing these data points leads to a substantially stronger negative correlation between $D_{d,m}$ and LWMR, changing the correlation coefficient from -0.36 to -0.61.

[33] The enhanced growth of large droplets following circulation mixing is similar to that of inhomogeneous mixing [*Baker et al.*, 1980] and entity-type entrainment mixing [*Telford and Chai*, 1980; *Telford et al.*, 1993]. In essence, the dilution of cloud parcels by clear, saturated air parcels reduces the concentration of cloud droplets. In the subsequent ascent, liquid water condenses on fewer droplets, and leads to enhanced droplet growth. The cycling of parcels also bears some resemblance to the entity-type entrainment mixing. *Baker et al.* [1980] postulated that inhomogeneous mixing proceeds as a two-step process. In the first step, all droplets in a portion of the cloud parcel evaporate to just saturate the dry air parcel being introduced from the surroundings at the same height. Then the remaining part of the cloud parcel is diluted by the saturated portion formed, which leads to a lower concentration of droplets but with the same size spectrum. *Baker et al.* [1980] applied this inhomogeneous mixing model to entrainment mixing from the sides of cumulus clouds and showed that the subsequent ascent of the mixed cloud parcel leads to larger droplets and a broader size spectrum, in qualitative agreement with observations [*Warner*, 1969]. For the stratocumulus cloud observed here, the mixing between entrained dry air and cloud parcel occurs mainly at the top of the cloud, and subsequent ascent of the cloud parcel after entrainment mixing is unlikely.

[34] In entity-type entrainment mixing [*Telford and Chai*, 1980; *Telford et al.*, 1993], droplet-free saturated air parcels generated as subsaturated turbulent entities from above the cloud top, also referred to as the turbules, mix with cloud air. During the descent of the turbules, the turbulence within the turbules keeps entrained cloud air well mixed, and all droplets evaporate before the tubule becomes saturated. After the tubule becomes saturated, further mixing of surrounding cloudy air into the clear saturated turbule leads to a droplet distribution which is the same as the surrounding cloud but with a reduced N_d. When buoyancy is restored with continued mixing, recycling upward begins, and the mixture with lower N_d leads to enhanced droplet growth in the same fashion as in both inhomogeneous mixing and circulation mixing described above. In fact, in circulation mixing, the mixing of an ascending subsaturated HLCL parcel (i.e., below its LCL at point B in Figure 8) with a LLCL cloud parcel may proceed through inhomogeneous mixing or a fashion similar to entity-type entrainment mixing (i.e., as a turbulent subsaturated entity), which results in fewer and larger droplets. The differences among these mixing mechanisms are related to their spatial scales. In entity-type entrainment mixing the recycling loop is

confined within the cloud and the upward journey begins at the same location where the descent ends. Circulation mixing, on the other hand, involves a loop that extends from the ocean surface to the top of the cloud, consistent with the coupled stratocumulus topped boundary layer [*Nicholls*, 1984], and the descent and ascent occur at different locations.

[35] Furthermore, evaporative cooling is suggested as one possible mechanism to start the descent of the turbule in entity-type entrainment mixing [*Telford et al.*, 1993]. However, observations [e.g., *Caughey et al.*, 1982; *Nicholls*, 1989] often suggest that the narrow descending regions within the stratocumulus clouds are probably a result of radiative cooling at the cloud top rather than evaporative cooling. During the G-1 flight on 27 July 2005, the air temperature above the cloud top was ~20°C, 7.5°C warmer than that at the highest in-cloud altitude (389 m), which was near the top of the cloud. The cloud parcel density after mixing with entrained clear air was calculated using the temperature and LWMR measured at the highest sampling level and the temperature and relative humidity measured above the cloud top over the full range of volume mixing ratios. The calculation shows that owing to the much warmer clear air above the cloud top, evaporative cooling alone was not sufficient to provide negative buoyancy to the mixed parcels. Therefore, entity-type entrainment mixing is unlikely to be driven by evaporative cooling in the stratocumulus cloud sampled. Circulation mixing is able to explain the enhanced growth of large droplets in parcels with low LWMR and is most consistent with the behavior of cloud microphysics observed during MASE.

5. Summary

[36] Marine stratocumulus microphysics is examined using airborne measurements conducted in the eastern Pacific off the coast of California in July 2005. During 3 days, aerosol concentrations were essentially uniform within the area of study so that the vertical distributions of cloud properties were purely a result of cloud microphysical processes; in addition, drizzle on each of the days was negligible. In-cloud measurements were made at a number of altitudes to obtain vertical profiles of cloud properties.

[37] On each of the 3 days, droplet number concentrations (N_d) averaged over each sampling altitude increased with altitude, while the interstitial aerosol concentration decreased with altitude. The average droplet mean diameter ($D_{d,m}$) increased with altitude, the average σ_{D_d} showed little variation with altitude, and the relative dispersion (ε) decreased with altitude. The correlation between $D_{d,m}$ and liquid water mixing ratio (LWMR) was positive at lower levels in cloud, but this correlation coefficient decreased with increasing distance above cloud base, becoming negative near cloud top. The minimum diameters defined by the largest 5 and 10 droplets cm^{-3} were also negatively correlated with LWMR at the upper levels in cloud, indicating enhanced growth of large droplets in cloud parcels with lower LWMR.

[38] The observations of cloud microphysics are consistent with a mechanism in which local cloud base height (LCBH) varies for parcels with different total water mixing ratios (TWMR). Sampling at higher altitudes includes less clear air (i.e., less likely below LCBH), which leads to higher average N_d and lower interstitial aerosol concentrations. The enhanced growth of large droplets and spectral broadening in parcels with low LWMR are consistent with a circulation mixing mechanism based on stratocumulus circulation. Ascending parcels exhibit a range of values of TWMR and lifting condensation level (LCL). When a parcel with low LCL (i.e., high TWMR) is diluted by another parcel at its higher LCL, both N_d and LWMR of the mixture are lower than those of the parcel with low LCL in the absence of mixing. During the subsequent ascent of the mixed parcel, small droplets form first on CCN originating in the parcel with higher LCL. Since the surface area of the newly formed droplets is considerably smaller than that of the already grown droplets that are originated in the low LCL parcel, the few large drops are the sites for preferential condensation and grow to sizes larger than those in the unmixed low LCL parcel. Both the formation of small droplets and the enhanced growth of large drops lead to broadening of the droplet spectrum. As a result, both σ_{D_d} and ε are negatively correlated with LWMR. The enhanced growth of large droplets following circulation mixing is similar to that of inhomogeneous mixing [*Baker et al.*, 1980] and entity-type entrainment mixing [*Telford and Chai*, 1980; *Telford et al.*, 1993]. The cycling of parcels also bears some resemblance to the entity-type entrainment mixing. Owing to the much warmer clear air above the cloud top during MASE, evaporative cooling alone was not sufficient to provide negative buoyancy to the mixed parcels, which is suggested to start the descent of "turbule" in "entity-type entrainment mixing" [*Telford et al.*, 1993]. The circulation mixing is most consistent with the behavior of cloud microphysics and meteorological conditions observed during MASE.

[39] The stratocumulus circulation mixing mechanism produces clouds with lower N_d and larger droplets, which lead to a lower cloud albedo at the same cloud LWP. Whereas the clouds sampled in the present study were essentially nondrizzling, the mechanism of circulation mixing is one that facilitates formation of precipitation embryos through both enhanced growth of large droplets and a broader cloud droplet spectrum. Continuous circulation mixing between cloudy and clear air can potentially generate droplets that are sufficiently large to initiate gravitational collection.

[40] **Acknowledgments.** The authors thank Steven Springston, who reduced the aircraft data used in this analysis, and the flight crew of the DOE Gulfstream-1 for their excellent work. We also thank two anonymous reviewers for their thoughtful and constructive comments. This research was sponsored by the Atmospheric Science Program within the Office of Biological and Environmental Research of U.S. Department of Energy under contract DE-AC02-98CH10886. Seong Soo Yum was also supported by the Korea Meteorological Administration Research and Development Program under grant CATER 2009-3214.

References

Albrecht, B. A. (1989), Aerosols, cloud microphysics, and fractional cloudiness, *Science*, *245*, 1227–1230, doi:10.1126/science.245.4923.1227.

Baker, M. B., R. G. Corbin, and J. Latham (1980), The influence of entrainment on the evolution of cloud droplet spectra. 1. A model of inhomogeneous mixing, *Q. J. R. Meteorol. Soc.*, *106*, 581–598, doi:10.1002/qj.49710644914.

Beard, K. V., and H. T. Ochs (1993), Warm-rain initiation: An overview of microphysical mechanisms, *J. Appl. Meteorol.*, *32*, 608–625, doi:10.1175/1520-0450(1993)032<0608:WRIAOO>2.0.CO;2.

Betts, A. K. (1978), Convection in the tropics, in *Meteorology Over the Tropical Ocean*, edited by D. B. Shaw, pp. 105–132, R. Meteorol. Soc., Reading, U. K.

Betts, A. K. (1983), Thermodynamics of mixed stratocumulus layers: Saturation point budgets, *J. Atmos. Sci.*, *40*, 2655–2670, doi:10.1175/1520-0469(1983)040<2655:TOMSLS>2.0.CO;2.

Brenguier, J. L. (1991), Parameterization of the condensation process: A theoretical approach, *J. Atmos. Sci.*, *48*, 264–282, doi:10.1175/1520-0469(1991)048<0264:POTCPA>2.0.CO;2.

Brenguier, J. L., and L. Chaumat (2001), Droplet spectra broadening in cumulus clouds. Part I: Broadening in adiabatic cores, *J. Atmos. Sci.*, *58*, 628–641, doi:10.1175/1520-0469(2001)058<0628:DSBICC>2.0.CO;2.

Brenguier, J. L., et al. (2000), Radiative properties of boundary layer clouds: Droplet effective radius versus number concentration, *J. Atmos. Sci.*, *57*, 803–821, doi:10.1175/1520-0469(2000)057< 0803:RPOBLC>2.0.CO;2.

Burnet, F., and J. L. Brenguier (2007), Observational study of the entrainment-mixing process in warm convective clouds, *J. Atmos. Sci.*, *64*, 1995–2011, doi:10.1175/JAS3928.1.

Caughey, S. J., B. A. Crease, and W. T. Roach (1982), A field-study of nocturnal stratocumulus. 2. Turbulence structure and entrainment, *Q. J. R. Meteorol. Soc.*, *108*, 125–144, doi:10.1002/qj.49710845508.

Chaumat, L., and J. L. Brenguier (2001), Droplet spectra broadening in cumulus clouds. Part II: Microscale droplet concentration heterogeneities, *J. Atmos. Sci.*, *58*, 642–654, doi:10.1175/1520-0469(2001)058<0642:DSBICC>2.0.CO;2.

Cooper, W. A. (1989), Effects of variable droplet growth histories on droplet size distributions. 1. Theory, *J. Atmos. Sci.*, *46*, 1301–1311, doi:10.1175/1520-0469(1989)046<1301:EOVDGH>2.0.CO;2.

Curry, J. A. (1986), Interactions among turbulence, radiation and microphysics in Arctic stratus clouds, *J. Atmos. Sci.*, *43*, 90–106, doi:10.1175/1520-0469(1986)043<0090:IATRAM>2.0.CO;2.

Duynkerke, P. G., H. Q. Zhang, and P. J. Jonker (1995), Microphysical and turbulent structure of nocturnal stratocumulus as observed during ASTEX, *J. Atmos. Sci.*, *52*, 2763–2777, doi:10.1175/1520-0469(1995)052<2763:MATSON>2.0.CO;2.

Gerber, H., B. G. Arends, and A. S. Ackerman (1994), New microphysics sensor for aircraft use, *Atmos. Res.*, *31*(4), 235–252, doi:10.1016/0169-8095(94)90001-9.

Gerber, H., G. Frick, S. P. Malinowski, J. L. Brenguier, and F. Burnet (2005), Holes and entrainment in stratocumulus, *J. Atmos. Sci.*, *62*, 443–459, doi:10.1175/JAS-3399.1.

Haman, K. E., et al. (2007), Small scale mixing processes at the top of a marine stratocumulus—A case study, *Q. J. R. Meteorol. Soc.*, *133*, 213–226, doi:10.1002/qj.5.

Hudson, J. G., and H. G. Li (1995), Microphysical contrasts in Atlantic stratus, *J. Atmos. Sci.*, *52*, 3031–3040, doi:10.1175/1520-0469(1995)052<3031:MCIAS>2.0.CO;2.

Hudson, J. G., and G. Svensson (1995), Cloud microphysical relationships in California marine stratus, *J. Appl. Meteorol.*, *34*, 2655–2666, doi:10.1175/1520-0450(1995)034<2655:CMRICM>2.0.CO;2.

Hudson, J. G., and S. S. Yum (1997), Droplet spectral broadening in marine stratus, *J. Atmos. Sci.*, *54*, 2642–2654, doi:10.1175/1520-0469(1997)054<2642:DSBIMS>2.0.CO;2.

Johnson, D. B. (1982), The role of giant and ultra-giant aerosol-particles in warm rain initiation, *J. Atmos. Sci.*, *39*, 448–460, doi:10.1175/1520-0469(1982)039<0448:TROGAU>2.0.CO;2.

Lu, M. L., W. C. Conant, H. H. Jonsson, V. Varutbangkul, R. C. Flagan, and J. H. Seinfeld (2007), The Marine Stratus/Stratocumulus Experiment (MASE): Aerosol-cloud relationships in marine stratocumulus, *J. Geophys. Res.*, *112*, D10209, doi:10.1029/2006JD007985.

Martin, G. M., D. W. Johnson, and A. Spice (1994), The measurement and parameterization of effective radius of droplets in warm stratocumulus clouds, *J. Atmos. Sci.*, *51*, 1823–1842, doi:10.1175/1520-0469(1994)051<1823:TMAPOE>2.0.CO;2.

Mason, B. J., and P. R. Jonas (1974), Evolution of droplet spectra and large droplets by condensation in cumulus clouds, *Q. J. R. Meteorol. Soc.*, *100*, 23–38, doi:10.1002/qj.49710042304.

McGraw, R., and Y. G. Liu (2006), Brownian drift-diffusion model for evolution of droplet size distributions in turbulent clouds, *Geophys. Res. Lett.*, *33*, L03802, doi:10.1029/2005GL023545.

Nicholls, S. (1984), The dynamics of stratocumulus: Aircraft observations and comparisons with a mixed layer model, *Q. J. R. Meteorol. Soc.*, *110*, 783–820, doi:10.1002/qj.49711046603.

Nicholls, S. (1989), The structure of radiatively driven convection in stratocumulus, *Q. J. R. Meteorol. Soc.*, *115*, 487–511, doi:10.1002/qj.49711548704.

Pawlowska, H., and J. L. Brenguier (2000), Microphysical properties of stratocumulus clouds during ACE-2, *Tellus, Ser. B*, *52*, 868–887, doi:10.1034/j.1600-0889.2000.00076.x.

Pawlowska, H., W. W. Grabowski, and J. L. Brenguier (2006), Observations of the width of cloud droplet spectra in stratocumulus, *Geophys. Res. Lett.*, *33*, L19810, doi:10.1029/2006GL026841.

Politovich, M. K. (1993), A study of the broadening of droplet size distributions in cumuli, *J. Atmos. Sci.*, *50*, 2230–2244, doi:10.1175/1520-0469(1993)050<2230:ASOTBO>2.0.CO;2.

Randall, D. A., et al. (1984), Outlook for research on sub-tropical marine stratiform clouds, *Bull. Am. Meteorol. Soc.*, *65*, 1290–1301, doi:10.1175/1520-0477(1984)065<1290:OFROSM>2.0.CO;2.

Robinson, N. F. (1984), The efficient numerical calculation of condensational cloud droplet growth, *J. Atmos. Sci.*, *41*, 698–700, doi:10.1175/1520-0469(1984)041<0698:TENCOC>2.0.CO;2.

Rogers, R. R., and M. K. Yau (1989), *A Short Course in Cloud Physics*, 3rd ed., Pergamon, Oxford, U. K.

Schubert, W. H., J. S. Wakefield, E. J. Steiner, and S. K. Cox (1979), Marine stratocumulus convection.1. Governing equations and horizontally homogeneous solutions, *J. Atmos. Sci.*, *36*, 1286–1307, doi:10.1175/1520-0469(1979)036<1286:MSCPIG>2.0.CO;2.

Sedunov, Y. S. (1974), *Physics of Drop Formation in the Atmosphere*, 234 pp., John Wiley, New York.

Shaw, R. A. (2003), Particle-turbulence interactions in atmospheric clouds, *Annu. Rev. Fluid Mech.*, *35*, 183–227, doi:10.1146/annurev.fluid.35.101101.161125.

Shaw, R. A., W. C. Reade, L. R. Collins, and J. Verlinde (1998), Preferential concentration of cloud droplets by turbulence: Effects on the early evolution of cumulus cloud droplet spectra, *J. Atmos. Sci.*, *55*, 1965–1976, doi:10.1175/1520-0469(1998)055<1965:PCOCDB>2.0.CO;2.

Srivastava, R. C. (1991), Growth of cloud drops by condensation: Effect of surface-tension on the dispersion of drop sizes, *J. Atmos. Sci.*, *48*, 1596–1605, doi:10.1175/1520-0469(1991)048<1596:GOCDBC>2.0.CO;2.

Strapp, J. W., W. R. Leaitch, and P. S. K. Liu (1992), Hydrated and dried aerosol-size distribution measurements from the FSSP-300 probe and the deiced PCASP-100X probe, *J. Atmos. Oceanic Technol.*, *9*, 548–555, doi:10.1175/1520-0426(1992)009<0548:HADASD>2.0.CO;2.

Telford, J. W., and S. K. Chai (1980), A new aspect of condensation theory, *Pure Appl. Geophys.*, *118*, 720–742, doi:10.1007/BF01593025.

Telford, J. W., K. E. Kim, T. S. Keck, and J. Hallett (1993), Entrainment in cumulus clouds. 2. Drop size variability, *Q. J. R. Meteorol. Soc.*, *119*, 631–653.

Twomey, S. (1974), Pollution and planetary albedo, *Atmos. Environ.*, *8*, 1251–1256, doi:10.1016/0004-6981(74)90004-3.

Twomey, S. (1977), Influence of pollution on shortwave albedo of clouds, *J. Atmos. Sci.*, *34*, 1149–1152, doi:10.1175/1520-0469(1977)034<1149:TIOPOT>2.0.CO;2.

Wang, J., Y.-N. Lee, P. H. Daum, J. Jayne, and M. L. Alexander (2008), Effects of aerosol organics on cloud condensation nucleus (CCN) concentration and first indirect aerosol effect, *Atmos. Chem. Phys. Discuss.*, *8*, 9783–9818.

Warner, J. (1969), Microstructure of cumulus cloud. I. General features of droplet spectrum, *J. Atmos. Sci.*, *26*, 1049–1059, doi:10.1175/1520-0469(1969)026<1049:TMOCCP>2.0.CO;2.

Warner, J. (1973), Microstructure of cumulus cloud. 4. Effect on droplet spectrum of mixing between cloud and environment, *J. Atmos. Sci.*, *30*, 256–261, doi:10.1175/1520-0469(1973)030<0256:TMOCCP>2.0.CO;2.

Weber, R. J., et al. (1998), Spurious aerosol measurements when sampling from aircraft in the vicinity of clouds, *J. Geophys. Res.*, *103*, 28,337–28,346, doi:10.1029/98JD02086.

Yum, S. S., and J. G. Hudson (2005), Adiabatic predictions and observations of cloud droplet spectral broadness, *Atmos. Res.*, *73*, 203–223, doi:10.1016/j.atmosres.2004.10.006.

P. H. Daum, Y. Liu, G. I. Senum, and J. Wang, Brookhaven National Laboratory, 75 Rutherford Drive, Upton, NY 11973-5000, USA. (jian@bnl.gov)

H. Jonsson, Center for Interdisciplinary Remotely Piloted Aircraft Studies, Naval Postgraduate School, Monterey, CA 93943, USA.

M.-L. Lu and J. H. Seinfeld, Department of Environmental Science and Engineering, California Institute of Technology, Pasadena, CA 91125, USA.

S. S. Yum, Department of Atmospheric Sciences, Yonsei University, Seoul 120-749, South Korea.